論文 / 著書情報
Article / Book Information

Citation	Hiroyoshi Tanabe, Shimpei Sato, Atsushi Takahashi "Fast EUV lithography simulation using convolutional neural network",Journal of Micro/Nanopatterning, Materials and Metrology (JM3),,(2021, 9),doi: https://doi.org/10.1117/1.JMM.20.4.041202
Copyright notice	Copyright 2021 Society of Photo-Optical Instrumentation Engineers (SPIE). One print or electronic copy may be made for personal use only. Systematic reproduction and distribution, duplication of any material in this paper for a fee or for commercial purposes, or modification of the content of the paper are prohibited.

Fast EUV lithography simulation using convolutional neural network

Hiroyoshi Tanabe,[a,*] Shimpei Sato,[b] and Atsushi Takahashi[a]
[a]Tokyo Institute of Technology, Tokyo, Japan
[b]Shinshu University, Nagano, Japan

Abstract

Background: Thin mask model has been conventionally used in optical lithography simulation. In extreme ultraviolet (EUV) lithography thin mask model is not valid because the absorber thickness is comparable to the mask pattern size. Rigorous electromagnetic (EM) simulations have been used to calculate the thick mask amplitudes. However, these simulations are highly time consuming.

Aim: Proposing a prototype of a convolutional neural network (CNN) which reduces the calculation time of rigorous EM simulations in a small mask area with specific mask patterns.

Approach: We construct a CNN which reproduces the results of the EM simulation. We define mask 3D amplitude as the difference between the thick mask amplitude and the thin mask amplitude. The mask 3D amplitude of each diffraction order is approximated using three parameters which represent the on-axis and the off-axis mask 3D effects. The mask 3D parameters of all diffraction orders are trained by a CNN.

Results: The input and the targets of the CNN are a cut-mask pattern and mask 3D parameters calculated by the EM simulation, respectively. After the training with 199,900 random cut-mask patterns, the CNN successfully predicts the mask 3D parameters of new cut-mask patterns.

Conclusions: We construct a CNN which predicts the diffraction amplitudes from 2D EUV mask patterns. After the training, the CNN successfully reproduces the mask 3D amplitude. CNN prediction is 5000 times faster than the rigorous EM simulation. Next challenge is to construct a practical CNN which covers a large area with general mask patterns.

 [DOI: 10.1117/1.JMM.20.4.041202]

Keywords: lithography simulation; neural network; extreme ultraviolet mask.

Paper 21031SS received Apr. 5, 2021; accepted for publication Jul. 20, 2021; published online Sep. 24, 2021.

1 Introduction

The adoption of extreme ultraviolet (EUV) lithography began in the mass production of logic and memory devices. Typical resolution of EUV lithography is 16 nm, assuming a moderate k_1 factor of 0.4. In this case, the minimum mask pattern size is 64 nm. Standard thickness of Ta absorber is around 60 nm and the aspect ratio of the mask pattern is nearly 1. High aspect absorber induces several mask 3D effects, such as critical dimension (CD) difference between horizontal and vertical lines and focus-dependent pattern shift.[1,2] Another example of the EUV mask 3D effect is the deviation of the phase-shift value near the absorber edges (Fig. 1). Due to the absorber edge effect, the optimum phase-shift value of an EUV phase shift mask is largely different from 180 deg.[3] Accurate EUV lithography simulations need to reproduce these mask 3D effects.

Rigorous electromagnetic (EM) simulation methods, such as finite-difference time-domain (FDTD) method,[4] rigorous coupled wave analysis,[5] and 3D waveguide model,[6] accurately calculate the mask 3D effects. However, these simulations are highly time consuming. Semi-

*Address all correspondence to Hiroyoshi Tanabe, tanabe.h.af@m.titech.ac.jp

1932-5150/2021/$28.00 © 2021 SPIE

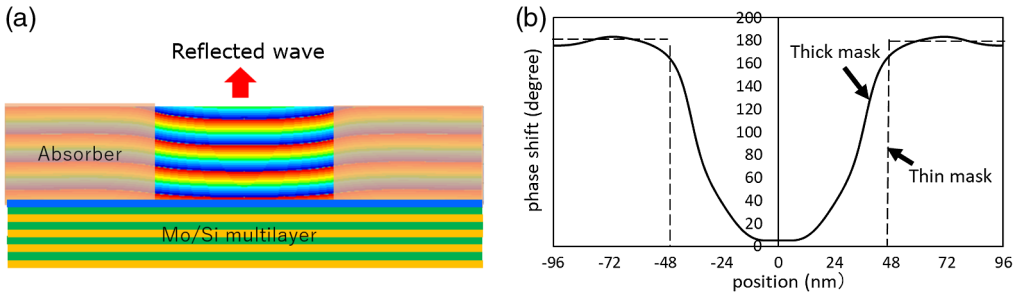

Fig. 1 (a) Reflected wave from an EUV mask and (b) its phase shift value at the surface of the absorber.

empirical and fast methods have been developed to include the mask 3D effects approximately in the calculation.[7–11] Recently with the advent of the deep learning software and hardware platforms, some attempts have been made to solve the mask 3D effect problems more accurately using deep neural networks.[12–14] The targets of the deep neural networks in these models are the near-field diffraction amplitudes of thick masks calculated by EM simulations. The near-field diffraction amplitudes are described in coordinated space and they oscillate locally. Also, these amplitudes vary depending on the incident angle of the illumination. It is not easy to model the incident angle dependence of the near-field diffraction amplitudes.

Our model also uses a deep neural network to accelerate the calculation of mask 3D effects. Here, we define the mask 3D amplitudes as the difference between the far-field diffraction amplitudes from a thick mask and those from a thin mask. The far-field diffraction amplitudes are described in pupil plane. They smoothly depend on the incident wave vector. In this study, we parametrize the mask 3D amplitudes linearly in the incident wave vector, which enables our model to be incorporated into transmission cross coefficient (TCC) method[15] and sum of coherent systems (SOCS) model[16] conventionally used in optical lithography simulations.

In Sec. 2, we explain the difference between the thin mask model and the thick mask model. We divide the thick mask amplitude into the thin mask amplitude and the mask 3D amplitude. In Sec. 3, we parametrize the mask 3D amplitude as functions of diffraction orders and source positions. In Sec. 4, we construct a convolutional neural network (CNN) which predicts the mask 3D amplitude. In Sec. 5, we extend the TCC method to include the mask 3D effects.

2 Thin Mask Model and Thick Mask Model

In this section, we treat the light as a scalar field to explain the concept of the mask 3D amplitude. In Sec. 3, we rigorously treat the light as a vector field.

Figure 2 shows the schematic view of partial-coherent lithography optics. The deep ultraviolet optics is shown here, but the basic system is the same for the EUV optics. The light emitted from the secondary source at the position (s_x, s_y) illuminates the mask from the oblique

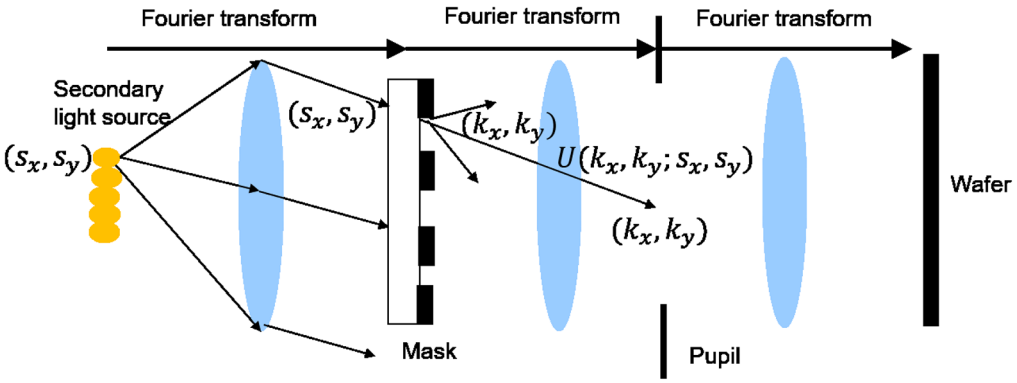

Fig. 2 Schematic view of partial-coherent lithography optics.

direction. The source position is Fourier transformed in the direction of the incident light by the condenser lens. The incident light has wave vector (s_x, s_y). The z component of the wave vector is calculated by the energy conservation law.

The incident light is diffracted from the mask. The diffracted light has wave vector (k_x, k_y). The amplitude of the diffracted light is $U(k_x, k_y; s_x, s_y)$. The diffracted light passes the pupil at the position (k_x, k_y). The pupil cuts the high-frequency components of the diffracted light. Then the diffracted light which passes the pupil forms an image on the wafer.

Total image intensity is the incoherent sum of the image intensities formed by the light emitted from all positions of the secondary light source. The total image intensity I is calculated by the following formula which is often called as Abbe's theory:

$$I(x,y) = \iint S(s_x, s_y) \left| \iint U(k_x, k_y; s_x, s_y) P(k_x, k_y) e^{-i(k_x x + k_y y)} \mathrm{d}k_x \, \mathrm{d}k_y \right|^2 \mathrm{d}s_x \, \mathrm{d}s_y, \quad (1)$$

where S is the source intensity and P is the pupil function. The key point of this formula is how to calculate the far-field diffraction amplitude $U(k_x, k_y; s_x, s_y)$.

Thin mask model is conventionally used in optical lithography simulation. The assumption of the model is that the near-field amplitude $U^{\mathrm{thin}}(x, y; s_x, s_y)$ is the product of the incident wave and the mask transmission function M [see Eq. (40) in Sec. 10.6 of Ref. 15].

$$U^{\mathrm{thin}}(x, y; s_x, s_y) = M(x, y) e^{i(s_x x + s_y y)}. \quad (2)$$

As shown in Ref. 15, TCC formula is derived by adapting Hopkins' method with the thin mask model.

In pupil plane, the far-field diffraction amplitude is written as follows:

$$U^{\mathrm{thin}}(k_x, k_y; s_x, s_y) = \frac{1}{(2\pi)^2} \iint M(x, y) e^{i((s_x - k_x)x + (s_y - k_y)y)} \mathrm{d}x \, \mathrm{d}y = M^{\mathrm{FT}}(k_x - s_x, k_y - s_y), \quad (3)$$

where M^{FT} is the Fourier transform of the mask transmission function. In thin mask model, the diffraction amplitude is calculated easily by Fourier transformation (FT) of the mask transmission function.

Equations (2) and (3) are not valid in thick mask model (Fig. 3). Rigorous EM simulation is required to calculate the diffracted wave accurately. In thick mask model, the diffraction amplitude U differs from the Fourier transform of the mask transmission function M^{FT} due to the mask 3D effect.

$$U(k_x, k_y; s_x, s_y) = M^{\mathrm{FT}}(k_x - s_x, k_y - s_y) + U^{\mathrm{3D}}(k_x, k_y; s_x, s_y). \quad (4)$$

This equation defines the mask 3D amplitude U^{3D}.

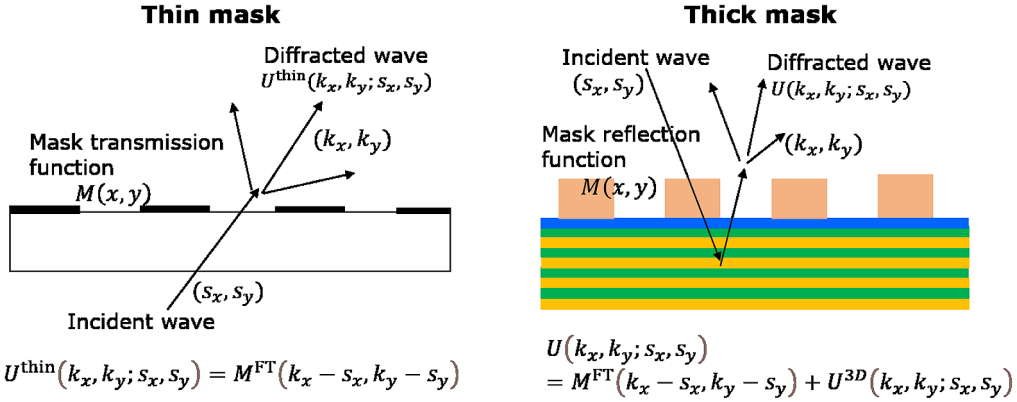

Fig. 3 Schematic views of a thin mask and a thick mask.

In thick mask model, we need to modify TCC formula because we cannot use Eq. (2). We discuss the details in Sec. 5.

3 Parameterization of the Mask 3D Amplitude

In this section, we treat the light rigorously as an EM vector field. One of the difficulties in the formulation of the 3D EM simulation is the number of the variables. The electric field has three components E_x, E_y, and E_z while the light has only two polarizations. Therefore, one of the three electric field components is redundant to parametrize the EM field. 3D waveguide model[6] uses the vector potential instead of the EM field. The model contains only two variables A_x and A_y which correspond to two polarizations. In the model, A_z is fixed to be zero after gauge transformation. The detail of A_x and A_y polarizations is explained in the Appendix.

Figure 4 shows a schematic view of light diffraction by an EUV mask. The light emitted from the secondary source illuminates the mask with the incident wave vector (s_x, s_y). Since EUV lithography uses reflective optics, the incident wave vector is defined by the difference from the wave vector at the chief-ray angle. The light is diffracted by the mask and the outgoing wave vector is (k_x, k_y). The scattering vector $(k_x - s_x, k_y - s_y)$ is the difference between the outgoing wave vector and the incident wave vector.

Similar to Eq. (4), the diffraction amplitude $\boldsymbol{A}$ of a thick mask is decomposed into the thin mask amplitude $\boldsymbol{A}^{\mathrm{FT}}$ and the mask 3D amplitude $\boldsymbol{A}^{\mathrm{3D}}$.

$$\boldsymbol{A}(k_x, k_y; s_x, s_y) = \boldsymbol{A}^{\mathrm{FT}}(k_x - s_x, k_y - s_y) + \boldsymbol{A}^{\mathrm{3D}}(k_x, k_y; s_x, s_y). \tag{5}$$

The thin mask amplitude $\boldsymbol{A}^{\mathrm{FT}}$ is calculated by the FT of the mask pattern using the reflection coefficients of the absorber and the multilayer. It depends only on the scattering vector. The mask 3D amplitude $\boldsymbol{A}^{\mathrm{3D}}$ is defined as the difference between the thick mask amplitude $\boldsymbol{A}$ and the thin mask amplitude $\boldsymbol{A}^{\mathrm{FT}}$. The mask 3D amplitude depends on the incident wave vector, which causes off-axis mask 3D effects described later.

The EM calculation of the thick mask amplitude is heavy. In this study, we use 3D waveguide model[6] to calculate the thick mask amplitude. We assume a periodic boundary condition with the mask pattern pitch L (Fig. 5). In this case, the scattering vector has a discrete value,

$$k_x - s_x = l\frac{2\pi}{L}, \quad k_y - s_y = m\frac{2\pi}{L}, \tag{6}$$

where (l, m) represents the diffraction order. For convenience, we also discretize the incident wave vector as follows:

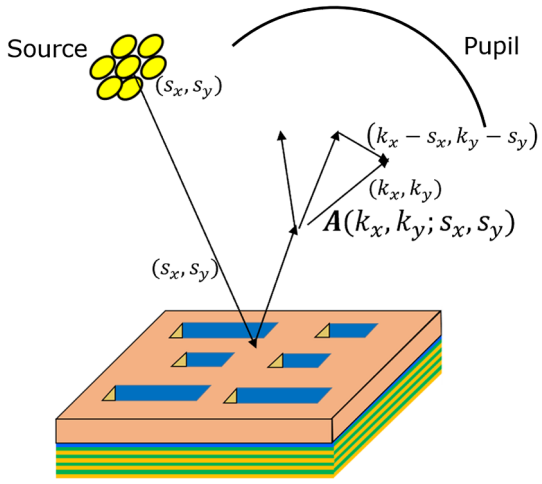

Fig. 4 Schematic view of light diffraction by an EUV mask.

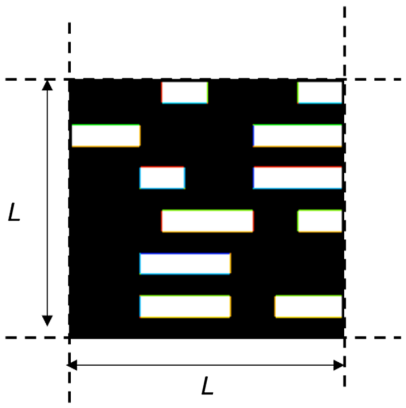

Fig. 5 Periodic mask pattern.

$$s_x = l_s \frac{2\pi}{L}, \quad s_y = m_s \frac{2\pi}{L}, \tag{7}$$

where (l_s, m_s) corresponds to the source position or incident angle. The pupil position or outgoing angle is specified by $(l + l_s, m + m_s)$. After the discretization of the wave vector, Eq. (5) is rewritten as follows:

$$\boldsymbol{A}(l, m; l_s, m_s) = \boldsymbol{A}^{\mathrm{FT}}(l, m) + \boldsymbol{A}^{\mathrm{3D}}(l, m; l_s, m_s). \tag{8}$$

All the elements of the thick mask amplitude are calculated simultaneously in 3D waveguide model. If we use FDTD method, we need to repeat the calculation for each incident angle.

The diffraction amplitude depends on four numbers, the diffraction order (l, m) and the source position (l_s, m_s). These numbers are restricted by the source shape and the pupil shape. Assuming the maximum σ value of the source shape to be 1, the source position is limited by the following equation:

$$\sqrt{l_s^2 + m_s^2} \leq \frac{\mathrm{NA}}{4} \frac{L}{\lambda}, \tag{9}$$

where $\mathrm{NA} = 0.33$ is the numerical aperture of the projection optics and $\lambda = 13.5$ nm is the wavelength. The magnification of the projection optics is 1/4. In the same way, the pupil shape limits the pupil position $(l + l_s, m + m_s)$ as follows:

$$\sqrt{(l + l_s)^2 + (m + m_s)^2} \leq \frac{\mathrm{NA}}{4} \frac{L}{\lambda}. \tag{10}$$

Figure 6 shows the graphical representation of the diffraction amplitude. The polarization of both the incident and outgoing waves is A_x. The circle at the center of the graph corresponds to the diffraction order $(l, m) = (0, 0)$. The peak value is 0.44 (the incident electric field amplitude is normalized to 1) and it is the largest among all diffraction orders. The right-side figure enlarges the amplitude at the diffraction order $(l, m) = (2, 2)$. The amplitude depends on the source position (l_s, m_s), which implies the incident angle dependence of the diffraction amplitude.

Figure 7 shows the polarization dependence of the diffraction amplitude. There are four combinations of the polarization of the incident wave and that of the outgoing wave. The polarization change after diffraction is very small for EUV masks. For example, the maximum value of the diffraction amplitude from A_x to A_x polarization is 0.44 while the maximum value from A_x to A_y polarization is 0.006. The result is not obvious, but this is probably because the EUV absorber has a refractive index close to 1. In the following discussion, we focus on the diffraction amplitude from A_x to A_x polarization. The light intensity is the square of the amplitude and we ignore the intensity from A_x to A_y polarization.

When the incident light is unpolarized, the image intensity is the average of the two intensities with two incident polarizations A_x and A_y. As shown in Fig. 7, the diffraction amplitude

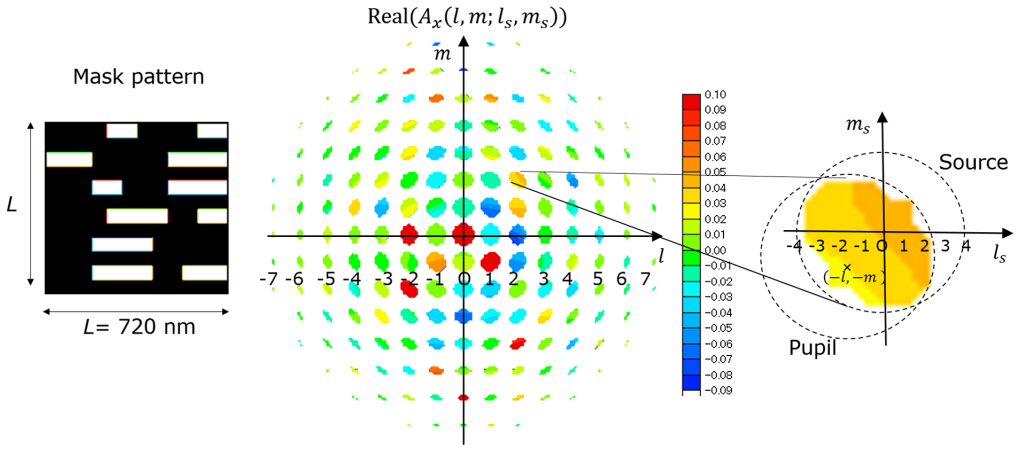

Fig. 6 Graphical representation of the diffraction amplitude.

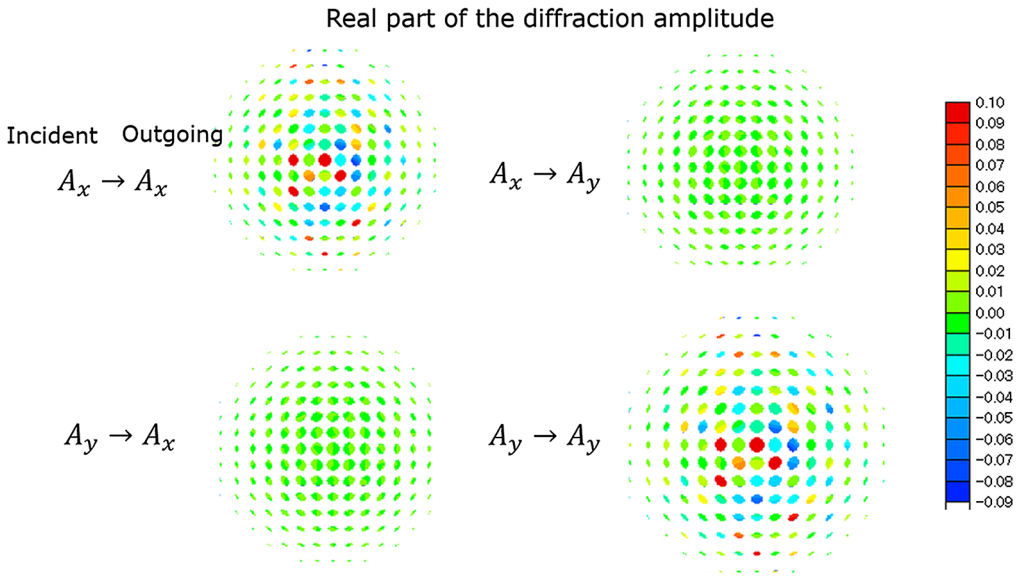

Fig. 7 Polarization dependence of the diffraction amplitude.

from A_y to A_y polarization is close to that from A_x to A_x polarization. In this study, we use same values for these two amplitudes, so the averaging is not required. It may be necessary to consider the difference between the two diffraction amplitudes in high NA optics.

According to Eq. (8), the thick mask amplitude is divided into the thin mask amplitude and the mask 3D amplitude. The contribution of the thin mask amplitude is dominant as shown in Fig. 8(b). The amplitude does not depend on the source position. It is calculated from the FT of the mask pattern assuming that the absorber area has the reflection coefficient of the absorber and the open area has the reflection coefficient of the multilayer.

The contribution of the mask 3D amplitude is small but not negligible as shown in Fig. 8(c). The amplitude gradually changes depending on the source position (l_s, m_s). We parametrize the mask 3D amplitude at each diffraction order (l, m) as a linear function of the source position (l_s, m_s).

$$A_x^{3D}(l, m; l_s, m_s) \cong a_0(l, m) + a_x(l, m) \cdot l_s + a_y(l, m) \cdot m_s, \tag{11}$$

where a_0 is the on-axis mask 3D amplitude at the center of the source plane. Both a_x and a_y are the slopes of the amplitude in the x and y directions of the source plane, respectively. The second and third terms in Eq. (11) represent the off-axis mask 3D amplitude. We included here only the

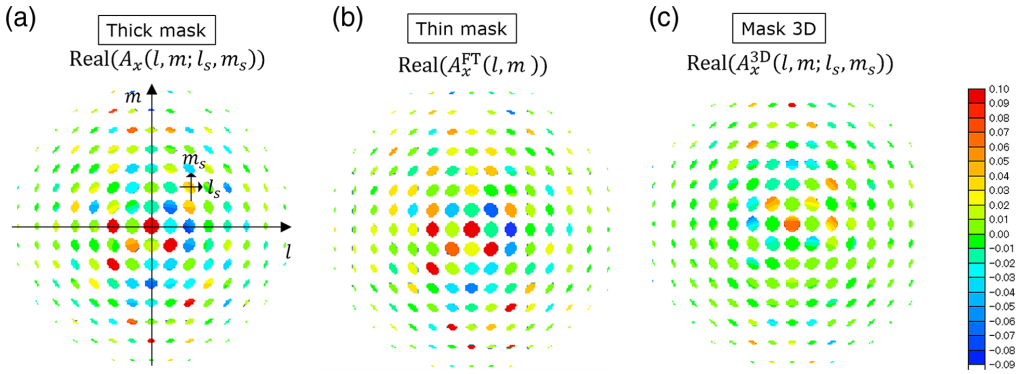

Fig. 8 Decomposition of the diffraction amplitude.

linear terms, but we can include higher terms if necessary. On the other hand, the linear terms may be unnecessary for large diffraction orders where the area of the possible source positions is small.

4 CNN for the Mask 3D Amplitude

The thin mask amplitude $A_x^{FT}(l,m)$ is the Fourier transform of the mask pattern and it can be calculated very fast. The mask 3D amplitude $A_x^{3D}(l,m;l_s,m_s)$ is calculated using the 3D waveguide model but the speed is slow. We characterize the mask 3D amplitude by three parameters a_0, a_x, and a_y. It is obvious that these mask 3D parameters are functions of the input mask pattern. We construct a CNN which reproduces the mask 3D parameters. We expect that the CNN calculation is much faster than the EM simulation.

The architecture of our CNN is shown in Fig. 9. Keras on TensorFlow is used for the deep learning software. The input mask pattern has 720×720 binary data. We first convert them to 72×72 grayscale numbers by averaging the data. This is the input to the CNN. Inside the CNN, we repeat convolutions and maxpoolings three times. Outputs of the CNN are the real and imaginary parts of a_0, a_x, and a_y. As shown in Fig. 9, for large diffraction orders, we parametrize the amplitude with a_0 only because the area representing possible source positions is small. In total, there are 1030 targets for CNN.

For training data, we generated 199,900 random horizontal cut-mask patterns [Fig. 10(a)].[17] The pattern pitch is 120 nm on the mask. The space width is 60 nm, and the space length has a

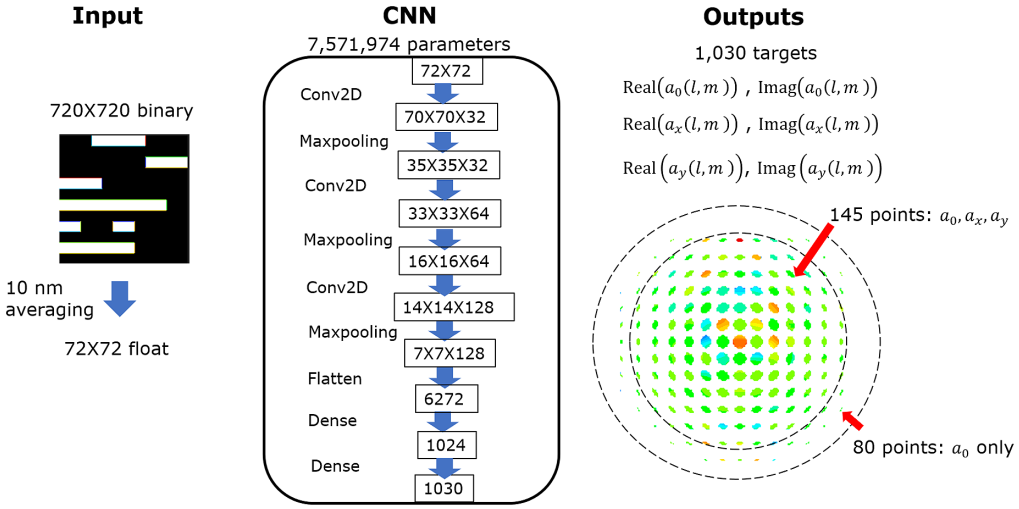

Fig. 9 Architecture of our CNN.

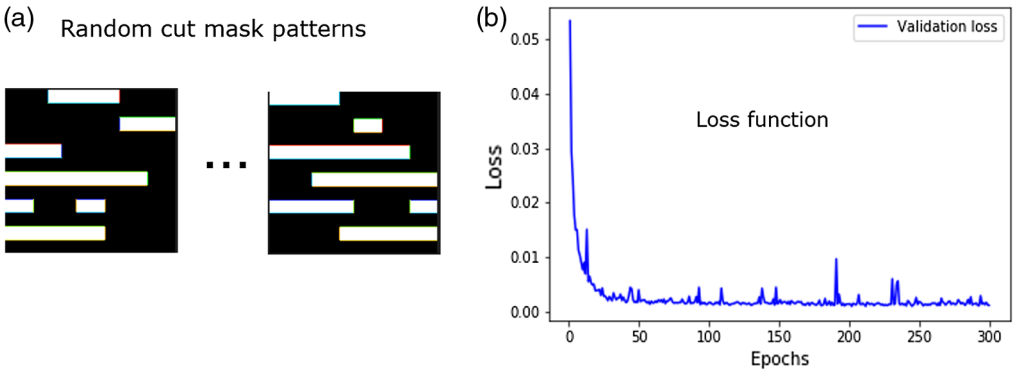

Fig. 10 Training and verification of our CNN. (a) Input mask patterns and (b) loss function during training.

random number between 120 and 600 nm. The fitting error decreased rapidly during the training [Fig. 10(b)]. The training time was about 10 hours.

After the training, we verified our CNN with 100 new data. Figure 11 compares the mask 3D parameters of 100 data at several diffraction orders calculated by EM simulation and the parameters predicted by CNN. The correlation between the parameters by EM simulation and CNN prediction is quite good. The correlation coefficient R^2 is more than 0.99 except for the parameter Real$(a_x(0,0))$. However, the value of this parameter is negligibly small compared to the

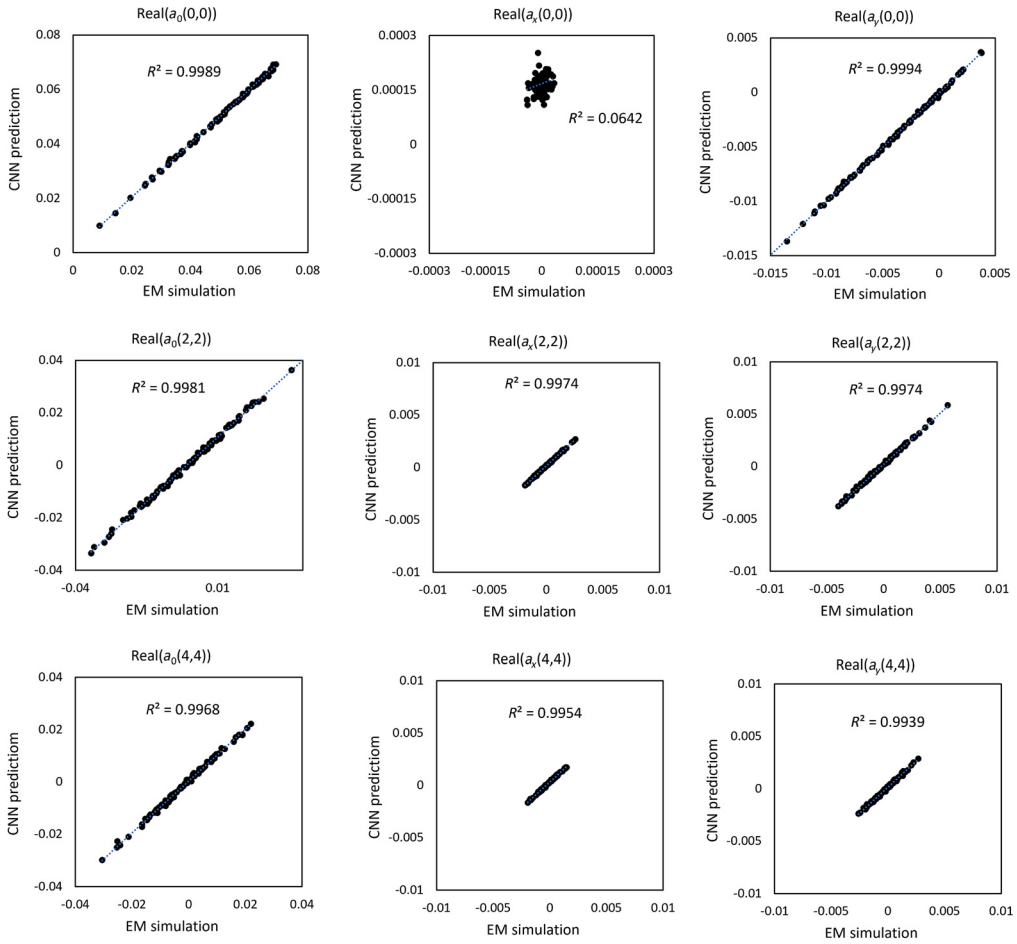

Fig. 11 Mask 3D parameters calculated by EM simulation and parameters predicted by CNN.

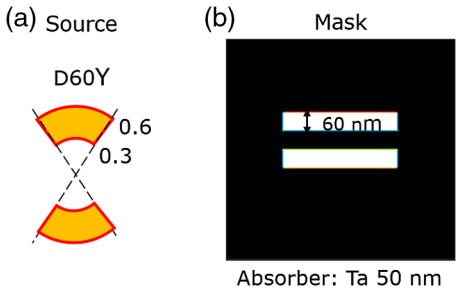

Fig. 12 Simulation conditions of a horizontal two-bar: (a) source shape and (b) mask pattern.

values of other parameters. This means that the zeroth-order reflected amplitude is almost independent of the azimuth angle of the incident wave.

We compare two examples of the wafer image intensities calculated by EM simulation, CNN, and FT. The first example is a horizontal two-bar in Fig. 12. It is well known that the mask 3D effect causes CD difference between two horizontal spaces at defocus positions, which is called two-bar CD asymmetry.[2] Figure 13 shows the results of the wafer image intensity calculations. The wavelength is 13.5 nm and NA is 0.33. CNN successfully reproduces the two-bar CD asymmetry. Thin mask model (FT) does not show CD asymmetry at defocus positions. The right-bottom figure shows the result of CNN which excludes a_x and a_y parameters. CD asymmetry is not reproduced without the off-axis mask 3D amplitude.

The second example is a vertical two-bar with both the source shape and mask pattern in Fig. 12 rotated 90 deg. Figure 14 shows the results of the wafer image intensity calculations. CNN fails to reproduce the result of EM simulation. This is expected because the training data of our CNN are horizontal cut-mask patterns. More study is needed to develop elaborated CNNs that can be applied to general mask patterns.

Figure 15 compares the computation time of the EM simulation and the prediction time of CNN. The computation time is the time to calculate the diffraction amplitudes and the prediction time is the time to predict the mask 3D parameters. Other steps such as the intensity integration and the FT are excluded. In this sense, the computation time of the thin mask model is zero. The computation time of the intensity integration and the FT depends on whether TCC formula and/or fast FT technique are used or not.

The most time-consuming part of the EM simulation is the large matrix calculation. Although the EM simulation does not use GPU, the matrix calculation is paralleled inside CPU by using Intel MKL. The computation time of the EM simulation linearly increased as a function of the number of the input data.

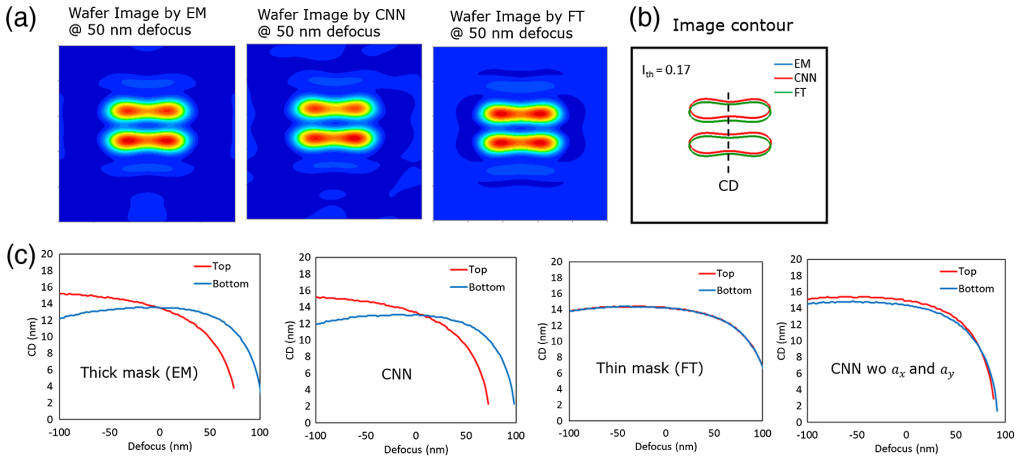

Fig. 13 (a) Wafer images, (b) image contours, and (c) focus dependence of CDs by EM simulation, CNN prediction, and FT calculation.

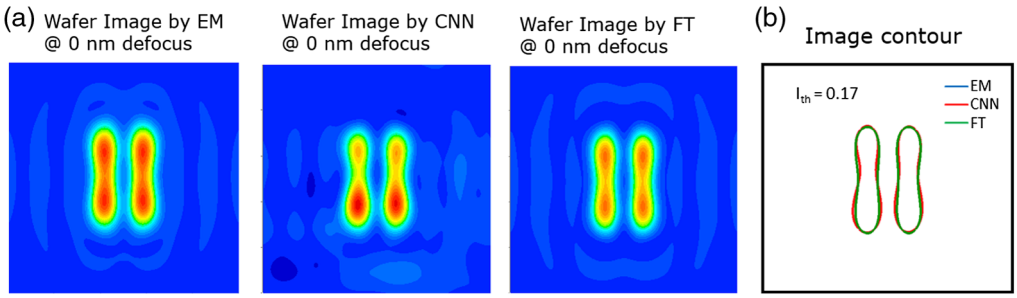

Fig. 14 (a) Wafer images and (b) image contours by EM simulation, CNN prediction, and FT calculation.

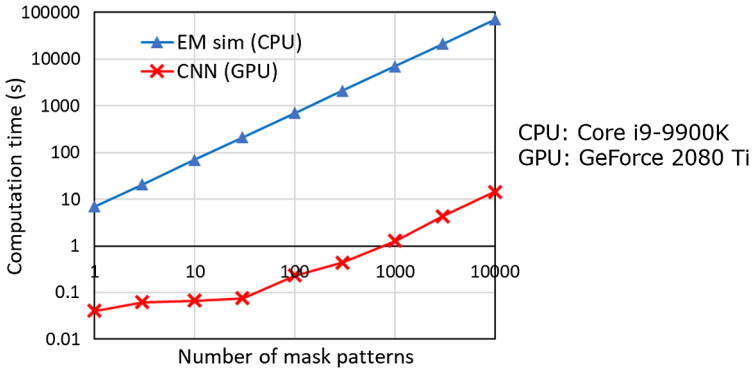

Fig. 15 Comparison of the computation time of the diffraction amplitudes.

CNN prediction uses GPU. To get the full performance of GPU, the number of the input data needs to be large. Computation time increases linearly beyond 300 input data. In this region, the CNN prediction is 5000 times faster than the EM simulation.

5 Extended TCC Formula

SOCS model is often used in optical lithography simulation, especially in optical proximity correction. The model decomposes TCC into a small number of eigen modes to accelerate the calculation. However, TCC formula is based on the thin mask model and the formula needs to be extended when the thick mask model is used. We first rewrite the mask 3D amplitude in Eq. (11) into the following wave vector form:

$$\boldsymbol{A}^{3D}(\boldsymbol{k};\boldsymbol{s}) \cong \boldsymbol{A}^{3D}(\boldsymbol{k}-\boldsymbol{s}) + \partial_{sx}\boldsymbol{A}^{3D}(\boldsymbol{k}-\boldsymbol{s})s_x + \partial_{sy}\boldsymbol{A}^{3D}(\boldsymbol{k}-\boldsymbol{s})s_y. \tag{12}$$

As shown in Eq. (5), the thick mask amplitude is the sum of the thin mask amplitude and the mask 3D amplitude.

$$\boldsymbol{A}(\boldsymbol{k};\boldsymbol{s}) = \boldsymbol{A}^{FT}(\boldsymbol{k}-\boldsymbol{s}) + \boldsymbol{A}^{3D}(\boldsymbol{k};\boldsymbol{s}). \tag{13}$$

Next, we convert the vector potential to the electric field. In coordinate space, the electric field is calculated from the vector potential as follows:[6]

$$\boldsymbol{E}(\boldsymbol{x};\boldsymbol{s}) = ik\boldsymbol{A}(\boldsymbol{x};\boldsymbol{s}) + \frac{i}{k}\nabla_{\boldsymbol{x}}(\nabla_{\boldsymbol{x}} \cdot \boldsymbol{A}(\boldsymbol{x};\boldsymbol{s})). \tag{14}$$

In momentum space, the above equation is written as

$$\boldsymbol{E}(\boldsymbol{k};\boldsymbol{s}) = ik\boldsymbol{A}(\boldsymbol{k};\boldsymbol{s}) - \frac{i}{k}(\boldsymbol{k}\cdot\boldsymbol{A}(\boldsymbol{k};\boldsymbol{s}))\boldsymbol{k} \tag{15}$$

Inserting Eqs. (12) and (13) into Eq. (15), we obtain the following equation:

$$\boldsymbol{E}(\boldsymbol{k};\boldsymbol{s}) \cong \boldsymbol{E}(\boldsymbol{k}-\boldsymbol{s}) + \partial_{sx}\boldsymbol{E}(\boldsymbol{k}-\boldsymbol{s})s_x + \partial_{sy}\boldsymbol{E}(\boldsymbol{k}-\boldsymbol{s})s_y. \tag{16}$$

Finally, according to Eq. (1), the image intensity I is calculated from the electric field as follows:

$$\begin{aligned} I(\boldsymbol{x}) &= \iint S(\boldsymbol{s})\left|\iint \boldsymbol{E}(\boldsymbol{k};\boldsymbol{s})P(\boldsymbol{k})e^{-i\boldsymbol{k}\cdot\boldsymbol{x}}\mathrm{d}\boldsymbol{k}\right|^2\mathrm{d}\boldsymbol{s} \\ &\cong \iint S(\boldsymbol{s})\left|\iint (\boldsymbol{E}(\boldsymbol{k}-\boldsymbol{s}) + \partial_{sx}\boldsymbol{E}(\boldsymbol{k}-\boldsymbol{s})s_x + \partial_{sy}\boldsymbol{E}(\boldsymbol{k}-\boldsymbol{s})s_y)P(\boldsymbol{k})e^{-i\boldsymbol{k}\cdot\boldsymbol{x}}\mathrm{d}\boldsymbol{k}\right|^2\mathrm{d}\boldsymbol{s} \\ &= \iint S(\boldsymbol{s})\left|\iint (\boldsymbol{E}(\boldsymbol{k}) + \partial_{sx}\boldsymbol{E}(\boldsymbol{k})s_x + \partial_{sy}\boldsymbol{E}(\boldsymbol{k})s_y)P(\boldsymbol{k}+\boldsymbol{s})e^{-i\boldsymbol{k}\cdot\boldsymbol{x}}\mathrm{d}\boldsymbol{k}\right|^2\mathrm{d}\boldsymbol{s}. \end{aligned} \tag{17}$$

In the case of high NA optics, the pupil function is a matrix which changes the direction of the electric field from the entrance pupil to the exit pupil.[18] In this paper, we treat the pupil function as a scalar function because NA of the current EUV optics is 0.33.

By interchanging the order of the integrations in Eq. (17), we get the following equation:

$$\begin{aligned} I(\boldsymbol{x}) \cong &\iint \mathrm{TCC}(\boldsymbol{k};\boldsymbol{k}')\boldsymbol{E}(\boldsymbol{k})\cdot\boldsymbol{E}(\boldsymbol{k}')^* e^{-i(\boldsymbol{k}-\boldsymbol{k}')\cdot\boldsymbol{x}}\mathrm{d}\boldsymbol{k}\,\mathrm{d}\boldsymbol{k}' \\ &+ 2\,\mathrm{Re}\left\{\iint \mathrm{TCC}_x(\boldsymbol{k};\boldsymbol{k}')\boldsymbol{E}(\boldsymbol{k})\cdot\partial_{sx}\boldsymbol{E}(\boldsymbol{k}')^* e^{-i(\boldsymbol{k}-\boldsymbol{k}')\cdot\boldsymbol{x}}\mathrm{d}\boldsymbol{k}\,\mathrm{d}\boldsymbol{k}'\right\} \\ &+ 2\,\mathrm{Re}\left\{\iint \mathrm{TCC}_y(\boldsymbol{k};\boldsymbol{k}')\boldsymbol{E}(\boldsymbol{k})\cdot\partial_{sy}\boldsymbol{E}(\boldsymbol{k}')^* e^{-i(\boldsymbol{k}-\boldsymbol{k}')\cdot\boldsymbol{x}}\mathrm{d}\boldsymbol{k}\,\mathrm{d}\boldsymbol{k}'\right\}, \end{aligned} \tag{18}$$

where TCC is the conventional transmission cross coefficient,

$$\mathrm{TCC}(\boldsymbol{k};\boldsymbol{k}') = \iint S(\boldsymbol{s})P(\boldsymbol{k}+\boldsymbol{s})P^*(\boldsymbol{k}'+\boldsymbol{s})\mathrm{d}\boldsymbol{s}, \tag{19}$$

and TCC_x and TCC_y are the extended transmission cross coefficients which represent the off-axis mask 3D effect.

$$\mathrm{TCC}_x(\boldsymbol{k};\boldsymbol{k}') = \iint s_x S(\boldsymbol{s})P(\boldsymbol{k}+\boldsymbol{s})P^*(\boldsymbol{k}'+\boldsymbol{s})\mathrm{d}\boldsymbol{s}, \tag{20}$$

$$\mathrm{TCC}_y(\boldsymbol{k};\boldsymbol{k}') = \iint s_y S(\boldsymbol{s})P(\boldsymbol{k}+\boldsymbol{s})P^*(\boldsymbol{k}'+\boldsymbol{s})\mathrm{d}\boldsymbol{s}. \tag{21}$$

In Eq. (18), we neglect the term proportional to $|\partial_{sx}\boldsymbol{E}(\boldsymbol{k})s_x + \partial_{sy}\boldsymbol{E}(\boldsymbol{k})s_y|^2$ because the contribution is small.

TCC, TCC_x, and TCC_y are the Hermitian matrices. Therefore, we can use the eigen value decomposition method in the SOCS model. Our formula is applicable to arbitrary source shapes and defocus. We can accelerate the calculation by selecting small number of the eigen functions which have large eigen values.

6 Summary

Diffraction amplitudes from thick EUV masks are calculated using 3D waveguide model. The model contains two components of the vector potential, A_x and A_y, which represent two polarizations. There is no redundant variable in the model.

We define the mask 3D amplitude as the difference between the thick-mask and thin-mask diffraction amplitudes. We decompose the mask 3D amplitude into three parts. One is the on-axis mask 3D amplitude, and others are the off-axis mask 3D amplitudes in x and y directions which depend on the incident angle of the illumination.

We construct a CNN which predicts the diffraction amplitudes from 2D EUV mask patterns. After the training, the CNN successfully reproduce the mask 3D effect of a horizontal two-bar. CNN prediction is 5000 times faster than the EM simulation.

We extend the TCC formula to include the off-axis mask 3D effect. Our formula is applicable to arbitrary source shapes and defocus. There are three TCCs in the formula. All of them are Hermitian matrices and we can use the eigen value decomposition method to accelerate the calculation.

In this study, the mask area is small (720 nm × 720 nm) and the mask patterns are restricted to horizontal cut-mask patterns. It is a big challenge to construct a practical CNN which covers a large area with general mask patterns while keeping high accuracy.

This work is based on the prior SPIE proceedings papers.[19,20]

7 Appendix: A_x and A_y Polarizations in Vacuum

Inside vacuum, the electric field $\boldsymbol{E}$ and magnetic field $\boldsymbol{H}$ of the light with wave vector $\boldsymbol{k}$ are described using the vector potential $\boldsymbol{A}$ under the Lorenz gauge condition as follows:[6]

$$\boldsymbol{E} = ik\boldsymbol{A} - \frac{i}{k}(\boldsymbol{k}\cdot\boldsymbol{A})\boldsymbol{k}, \tag{23}$$

$$\boldsymbol{H} = i\boldsymbol{k}\times\boldsymbol{A}. \tag{24}$$

Wave vector, electric field, and magnetic field are perpendicular to each other.

$$\boldsymbol{E}\cdot\boldsymbol{k} = \boldsymbol{H}\cdot\boldsymbol{k} = \boldsymbol{E}\cdot\boldsymbol{H} = 0. \tag{25}$$

The magnitudes of the electric and the magnetic fields are the same.

$$|\boldsymbol{E}|^2 = |\boldsymbol{H}|^2 = k^2|\boldsymbol{A}|^2 - |\boldsymbol{k}\cdot\boldsymbol{A}|^2. \tag{26}$$

Gauge transformation freedom allows A_z to be fixed at zero when the media is uniform in z direction.[6] This gauge condition can be applied also in the vacuum. Therefore, two components of the vector potential, A_x and A_y, determine the EM field of the light. The vector potentials, electric fields, and magnetic fields of A_x and A_y polarizations are explicitly written as follows:

A_x polarization:

$$\boldsymbol{A} = (A_x, 0, 0), \tag{27}$$

$$\boldsymbol{E} = \frac{iA_x}{k}(k^2 - k_x^2, -k_y k_x, -k_z k_x), \tag{28}$$

$$\boldsymbol{H} = iA_x(0, k_z, -k_y). \tag{29}$$

A_y polarization:

$$\boldsymbol{A} = (0, A_y, 0), \tag{30}$$

$$\boldsymbol{E} = \frac{iA_y}{k}(-k_x k_y, k^2 - k_y^2, -k_z k_y), \tag{31}$$

$$\boldsymbol{H} = iA_y(-k_z, 0, k_x). \tag{32}$$

When the wave vector is in x-z plane, $k_y = 0$. In this case, A_x polarization corresponds to transverse magnetic (TM) polarization and A_y polarization corresponds to transverse electric (TE) polarization. In the same way, when the wave vector is in y-z plane, A_x polarization corresponds to TE polarization and A_y polarization corresponds to TM polarization.

When $k_x, k_y \ll k$, $\boldsymbol{E} \sim (ikA_x, 0, 0)$ for A_x polarization and $\boldsymbol{E} \sim (0, ikA_y, 0)$ for A_y polarization. The electric field of A_x polarization is almost parallel to the x-axis, and the electric field of A_y polarization is almost parallel to the y-axis.

References

1. A. Erdmann et al., "3D mask effects in high NA EUV imaging," *Proc. SPIE* **10957**, 109570Z (2019).
2. T. Last et al., "Illumination pupil optimization in 0.33NA EUVL by intensity balancing for semi-iso dark field two-bar M1 building blocks," *Proc. SPIE* **10032**, 100320A (2016).
3. M. C. Lare, F.J. Timmermans, and J. Finders, "Alternative reticles for low-k1 EUV imaging," *Proc. SPIE* **11147**, 111470D (2019).
4. A. Wong, "TEMPEST users' guide," UCB/ERL M94/64 (1994).
5. M. G. Moharam and T. K. Gaylord, "Rigorous coupled-wave analysis of planar-grating diffraction," *J. Opt. Soc. Am.* **71**, 811 (1981).
6. K. D. Lucas, H. Tanabe, and A. J. Strojwas, "Efficient and rigorous three-dimensional model for optical lithography simulation," *J. Opt. Soc. Am. A* **13**, 2187 (1996).
7. K. Adam and A. R. Neureuther, "Simplified modes for edge transitions in rigorous mask modeling," *Proc. SPIE* **4346**, 331 (2001).
8. A. Erdmann et al., "Efficient simulation of light from 3-dimensional EUV-masks using field decomposition techniques," *Proc. SPIE* **5037**, 482 (2003).
9. P. Liu et al., "Fast 3D thick mask model for full-chip EUVL simulations," *Proc. SPIE* **8679**, 86790W (2013).
10. H. Zhang et al., "A pattern- and optics-independent compact model of mask3D under off-axis illumination with significant efficiency and accuracy improvement," *Proc. SPIE* **9426**, 94260Q (2015).
11. V. Domnenko et al., "EUV computational lithography using accelerated topographic mask simulation," *Proc. SPIE* **10962**, 109620O (2019).
12. S. Lan et al., "Deep learning assisted fast mask optimization," *Proc. SPIE* **10587**, 105870H (2018).
13. P. Liu, "Mask synthesis using machine learning software and hardware platforms," *Proc. SPIE* **11327**, 1132707 (2020).
14. R. Pearman et al., "Fast all-angle mask 3D ILT patterning," *Proc. SPIE* **11327**, 113270F (2020).
15. M. Born and E. Wolf, *Principles of Optics*, 7th ed., Cambridge University Press, Cambridge (1999).
16. N. B. Cobb, "Fast optical and process proximity correction algorithms for integrated circuit manufacturing," PhD Dissertation, University of California, Berkeley (1998).
17. Y. Borodovsky, "EUV Lithography at insertion and beyond," in *Int. Workshop EUV Lithogr.* (2012).
18. M. S. Yeung et al., "Extension of the Hopkins theory of partially coherent imaging to include thin-film interference effects," *Proc. SPIE* **1927**, 452 (1993).
19. H. Tanabe, S. Sato, and A. Takahashi, "Fast 3D lithography simulation by convolutional neural network: POC study," *Proc. SPIE* **11518**, 115180L (2020).
20. H. Tanabe, S. Sato, and A. Takahashi, "Fast 3D lithography simulation by convolutional neural network," *Proc. SPIE* **11614**, 116140M (2021).

Hiroyoshi Tanabe is a researcher at Tokyo Institute of Technology. He received his PhD in physics from the University of Tokyo in 1986. He has more than 30 years of experience in optical

and EUV lithography. He is the author of more than 30 papers. He was the program committee chair of Photomask Japan in 2003 and 2004. His current research interests include EUV masks and lithography simulation. He is a member of SPIE.

Shimpei Sato received the BE, ME, and DE degrees in engineering from Tokyo Institute of Technology, Tokyo, Japan, in 2007, 2009, and 2014, respectively. He is currently an assistant professor in the Department of Electrical and Computer Engineering, Shinshu University. His current research interests include approximate computing realization by architecture design and circuit design and their applications. He is a member of IEEE, IEICE, and IPSJ.

Atsushi Takahashi received his BE, ME, and DE degrees in electrical and electronic engineering from Tokyo Institute of Technology, Tokyo, Japan, in 1989, 1991, and 1996, respectively. He is currently a professor in the Department of Information and Communications Engineering, School of Engineering, Tokyo Institute of Technology. His research interests are in VLSI layout design and combinational algorithms. He is a fellow of IEICE, a senior member of IEEE and IPSJ, and a member of ACM.